PERGAMON

International Journal of Solids and Structures 37 (2000) 4915–4931

INTERNATIONAL JOURNAL OF SOLIDS and STRUCTURES

www.elsevier.com/locate/ijsolstr

Influence of nonlinear boundary conditions on the single-mode response of a cantilever beam

Mahmood Tabaddor [1]

Department of Engineering Science and Mechanics, Virginia Polytechnic Institute and State University, Blacksburg, VA 24061-0219, USA

Received 18 September 1998; in revised form 8 July 1999

Abstract

In this paper, we compare the experimentally and theoretically obtained single-mode responses of a cantilever beam. The analytical portion involves solving an integro-differential equation via the method of multiple scales. For the single-mode response, a large discrepancy is found between theory and experiment for an assumed ideal clamp model. Through some experimental detective work, it was found, and later shown through analysis, that the substitution of a torsionally elastic end for the fixed support brought the theoretical and experimental results into excellent agreement. The torsional spring has both linear and nonlinear (cubic) stiffness components. © 2000 Elsevier Science Ltd. All rights reserved.

Keywords: Nonlinear; Cantilever beam; Flexible boundary

1. Introduction

In the study of structures, the modeling of boundary conditions, such as clamps, joints, and other connectors is difficult. In most analyses, the typical boundary conditions are free, sliding, clamped, and pinned. Of course, at times, these idealizations are bound to fall short and it then becomes necessary to raise the level of realism of the model. The most popular refinement of the classical boundary conditions is the substitution of rotational and translational springs to account for boundary flexibility (Gorman, 1975). Furthermore, damping elements and mass elements are added features that can improve the ability of a mathematical model to approximate the response of a structure.

The results presented here are an extension of a study (Tabaddor and Nayfeh, 1997) on the

E-mail address: mtabaddor@bell-labs.com (M. Tabaddor).

[1] *Present address*: Bell Labs, Lucent Technologies, 2000 NE Expressway, GA, 30071.

PII: S0020-7683(99)00197-3

multimode response of a cantilever beam near its fourth natural frequency. However, in this paper, we focus on the single-mode nonlinear response of a cantilever beam near its fourth natural frequency. As an outline, first we begin with a simple survey of applicable research followed by a description of the experimental setup. The succeeding sections detail the perturbation solution for a selected cantilever beam model, a comparison of experimentally and theoretically obtained results, and an investigation of the noted discrepancies. Finally, a revised theoretical model, that predicts the experimentally obtained results better by accounting for the elasticity of the boundary, is presented.

2. Literature review

In this section, a brief review of references in the English technical literature relevant to the dynamics of beams, mostly cantilever, is presented.

2.1. Theoretical modeling

Bypassing the complexity of a full three-dimensional elasticity analysis, Crespo da Silva and Glynn (1978a, 1978b) derived nonlinear integro-partial-differential equations governing the nonplanar dynamics of an isotropic, inextensional beam. The resulting equations, developed through the extended Hamilton's principle, retain all nonlinearities up to the third order. Therefore, contributions from both nonlinear curvature and nonlinear inertia were kept. The form of these equations allows for a solution based on perturbation analyses (Nayfeh, 1973, 1981). Pai and Nayfeh (1992) developed a more comprehensive beam theory, which fully accounts for geometric nonlinearities, including large rotations and displacements and shear deformation. Hodges (1984, 1987a, 1987b), Pai and Nayfeh (1990) and Nayfeh and Pai (1996) discussed the development of concepts in nonlinear beam kinematics. Hodges et al. (1988) discussed some of the common mistakes in the nonlinear modeling of a cantilever beam. Specifically, they addressed the issues of proper physical interpretation of the Euler angles and the failure to obtain equations consistent to the order of approximation being considered.

Simplifying assumptions are common in engineering theories of beams (Donnell, 1976; Love, 1944). They make the world easier to understand or, at least, to solve mathematically. Efforts to develop equations of motion describing the behavior of a beam in a manner that lend themselves to a viable solution have resulted in numerous modeling techniques (Boutaghou and Erdman, 1989; Haering et al., 1992; Nayfeh and Pai, 1996; Crespo da Silva, 1991). Each researcher attempts to improve the comprehensiveness of a model over previous models by accounting for various complicating effects, such as torsion, rotary inertia, shear center eccentricity, warping, axial stretching, and general deformations. The challenge is to include enough complexity so that the problem is meaningful and, yet, apply simplifying assumptions that make the problem tractable (Suleman et al., 1995).

The advent of the digital computer has no doubt played a hand in the progress of dynamic modeling. However, the use of numerical algorithms in the area of computational mechanics is not without its dangers and blind faith in numerical answers should be avoided (Oden and Bathe, 1978). Nevertheless, since for most nonlinear systems a closed-form solution is unattainable, recourse is made to perturbation methods (Nayfeh, 1973, 1981) and hybrid perturbation-numerical methods (Nayfeh et al., 1974; Nayfeh and Balachandran, 1995) for qualitative information about the solution space. A combined qualitative and quantitative analysis is the most reassuring strategy in the tackling of nonlinear problems.

2.2. Single-mode response

Nonlinear motions of beams vibrating in a manner essentially captured by a single mode were the focus of early works cited in Ref. (Nayfeh and Mook, 1979). The characteristics of bending of the frequency-response curve, amplitude jumps, limit cycles, and hysteresis are well documented for the case of a single mode under the influence of nonlinearity.

Dowell et al. (1977) compared linear and nonlinear theories with experiments for large deformations of a cantilever, metallic beam due to a tip load. They concluded that the experimental results for various frequency measurements were in close agreement with linear and nonlinear theories only for tip deflections that are not a significant fraction of the beam span.

Zavodney and Nayfeh (1989) compared experimental and analytical results for a parametrically excited cantilever, metallic beam with a lumped mass. Their theoretical model contained nonlinear terms up to the third order. The sources of the nonlinearities were the inertia, curvature, and axial displacement (produced by a large transverse deflection). They concentrated on single-mode planar motions. They experimentally documented jumps in the frequency-response curves for metallic and composite beams. The jump points varied with increasing acceleration levels. For the theoretical results, they relied on a discretization of the governing equation by Galerkin's method followed by the application of the method of multiple scales (Nayfeh, 1981) to obtain the time variation of the amplitude and phase of the motion as a function of the system and forcing parameters.

Anderson et al. (1996) experimentally observed that, for a primary excitation of the first mode of a cantilever, metallic beam, the curvature nonlinearity dominates the inertia nonlinearity. The resulting frequency-response curve is bent to the right, revealing hardening-type nonlinearity. For a primary excitation of the second mode, they found that the inertia nonlinearity dominates. In this case, the frequency-response curve is bent to the left and the nonlinearity is of a softening type.

Berdichevsky et al. (1995) analytically studied the nonlinear vibrations of a cantilever, isotropic beam excited at the free end. They found that, for a one-degree-of-freedom model, the dynamical response can be explained in terms of a dynamical potential.

Experimental studies by Moon and Holmes (1985) on the vibration of a buckled elastic beam found the existence of chaotic motions as the beam alternates between the two static equilibrium positions.

3. Experimental setup

Fig. 1 shows a schematic of the experimental setup for the vertically positioned beam. The beam was made of SAE 1095 steel with the dimensions 84.45 cm $\times$ 0.81 mm $\times$ 1.57 cm. It was mounted through a steel clamping fixture attached to a shaker. A signal generator in line with a power amplifier provided a harmonic input signal to the shaker. This allowed for manual control of the excitation frequency and amplitude. The output of the shaker was measured with an accelerometer placed on the clamping fixture, whereas the response of the cantilever beam was measured with a 350 Ω strain gage mounted approximately 2.54 cm from the fixed end of the horizontal beam. These signals were subsequently processed through an analog multi-channel low-pass filter set to a cut-off frequency of 500 Hz. This filter also allowed for AC coupling of the signals. The power spectra of the transducer signals were calculated in real time over a 40 Hz bandwidth (0.05 Hz frequency resolution) with a Hanning window using a dynamic signal analyzer. At points of interest, the data were converted digitally through an A/D card on a digital computer and stored for further characterization and processing.

For the beam, the investigation concentrated on a frequency range around the fourth natural frequency of the beam. Once the beam was mounted, the only two control parameters were the excitation frequency and amplitude. Sweeps were performed by varying either of these two parameters

while keeping the other fixed. These sweeps allowed for characterization of the nonlinear dynamics of the beam by capturing jumps and multiple solutions in a methodical manner. At each increment of the control parameter, we waited for a sufficiently long time, allowing for the transients to die away, before recording the response. The spectrum of the strain gage was the key component in determining whether a stationary state in the dynamics of the beam had been reached. Then, the magnitudes of the peaks in the response spectrum associated with the natural frequencies of the beam were recorded. The collection of such points produced the frequency- and amplitude-response curves that are shown in the results. The magnitudes of the strains (in volts) associated with each peak were scaled by the frequency of each peak to obtain a numerical measure that is proportional to the displacement. The calibration constant for the strain gage would be necessary to convert to the actual displacement. Though, for higher modes, dynamic calibration, using either an accelerometer or a laser vibrometer, is necessary (McConnell, 1995).

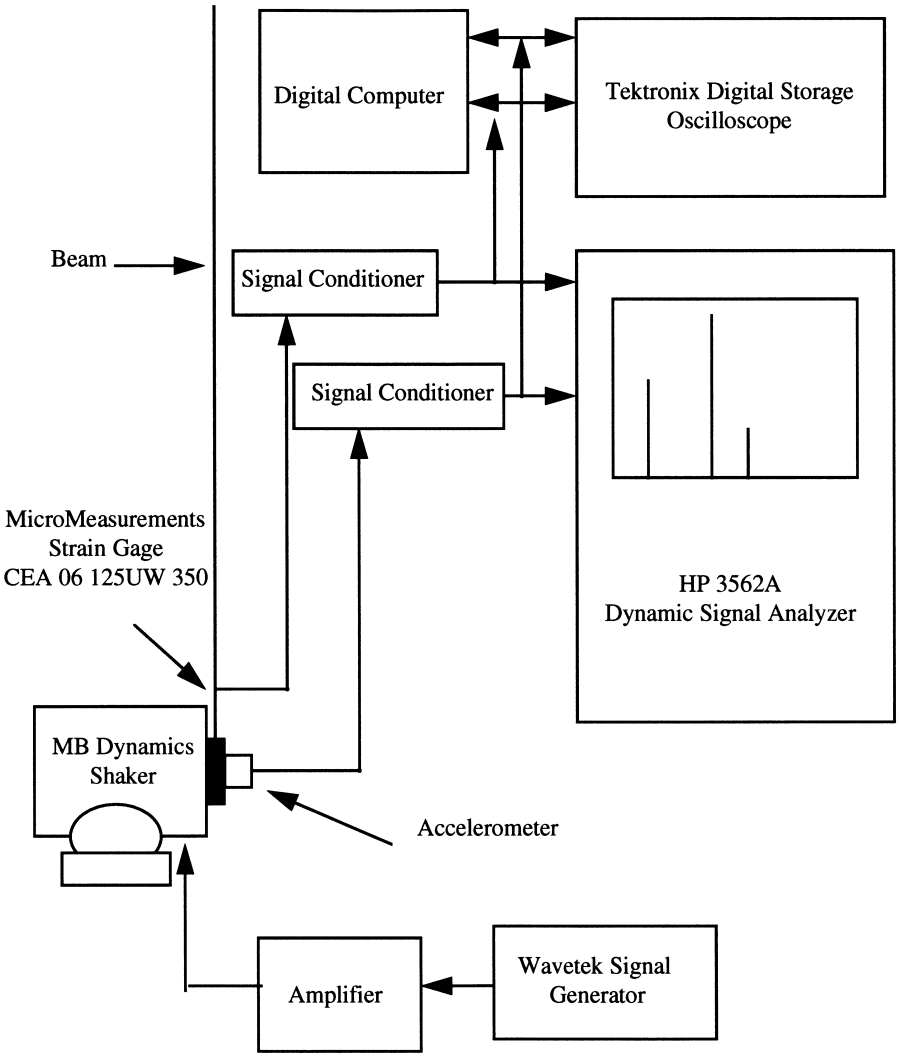

Fig. 1. A schematic of the experimental setup.

For our purposes, a measurement proportional to displacement is sufficient. All documented motions were observed to be planar.

4. Linear natural frequencies

The first step in any vibration study is the determination of the linear natural frequencies. They are then used as a starting point in the investigation of nonlinear phenomena. The natural frequencies of the beam were found experimentally by using the frequency-response function of the analyzer. The inputs processed included the accelerometer signal, measuring the amplitude of a random excitation, and the strain gage signal, measuring the induced strain. The placement of the strain gage was based on the need for a strong signal-to-noise ratio and the avoidance of being on or near the node of any of the vibration modes of interest. Peaks in the amplitude portion of the frequency-response function were associated with the linear natural frequencies of the beam. To increase confidence in the experimentally obtained natural frequencies, we measured the frequency-response functions at several low excitation levels. No noticeable shifts in the peaks were observed. Also, a periodic checking of the natural frequencies of the beam were performed to detect any fatigue damage (Ostachowicz and Krawczuk, 1991).

The linear natural frequencies of the cantilever beam in the vertical configuration are listed in Table 1. The Euler–Bernoulli values fail to accurately predict the first natural frequency. The agreement improves with each higher frequency for the first four natural frequencies. The discrepancy is due to the effect of gravity on the stiffness of the cantilever beam. The second column in Table 1 shows the results from an analysis incorporating the effect of gravity (Tabaddor, 1996)

5. Equation of motion

To study the nonlinear response of a cantilever beam, we apply the equations developed by Crespo da Silva and Glynn (1978a). These equations are simplified to the case of planar motion of a metallic uniform cantilever beam to an external harmonic excitation. In addition, we add at this early point a term quadratic in velocity and account for torsional flexibility of the clamped end in anticipation of their future need. The integro-differential equation, under assumptions outlined in Ref. (Crespo da Silva and Glynn, 1978a), then becomes

$$m\frac{\partial^2\hat{v}}{\partial\hat{t}^2}+\hat{\mu}\frac{\partial\hat{v}}{\partial\hat{t}}+EI\frac{\partial^4\hat{v}}{\partial\hat{s}^4}=-EI\frac{\partial}{\partial\hat{s}}\left\{\frac{\partial\hat{v}}{\partial\hat{s}}\frac{\partial}{\partial\hat{s}}\left[\frac{\partial\hat{v}}{\partial\hat{s}}\frac{\partial^2\hat{v}}{\partial\hat{s}^2}\right]\right\}-\frac{\partial}{\partial\hat{s}}\left\{\frac{1}{2}\int_L^{\hat{s}}m\frac{\partial^2}{\partial\hat{t}^2}\left[\int_0^{\hat{s}}\left(\frac{\partial\hat{v}}{\partial\hat{s}}\right)^2\mathrm{d}s\right]\mathrm{d}s\right\}$$
$$+m\hat{a}_b\cos(\hat{\Omega}\hat{t})-\hat{c}|\frac{\partial\hat{v}}{\partial\hat{t}}|\frac{\partial\hat{v}}{\partial\hat{t}}. \tag{1}$$

Table 1
Natural frequencies of a cantilever beam, Hz

Mode No.	Euler–Bernoulli	E.B. w/gravity	Experimental values
1	0.96	0.70	0.70
2	6.03	5.85	5.85
3	16.87	16.65	16.65
4	33.07	32.83	32.95

The variables are defined as follows: m is the mass per unit length, L is the beam length, E is Young's modulus, I is the area moment of inertia, $\hat{v}$ is the transverse displacement, $\hat{s}$ is the arclength, $\hat{t}$ is time, $\hat{a}_b$ is the acceleration of the supported end of the beam, $\hat{c}$ is the coefficient of quadratic damping, $\hat{\Omega}$ is the frequency of the support motion, and $\hat{\mu}$ is the linear viscous damping coefficient. Note that the displacement is a function of the arclength and time while all other variables are assumed to be constant.

The first two terms on the right-hand side of Eq. (1) are the *nonlinear* terms accounting for *curvature* and *inertia* effects, respectively. The third term is the harmonic external base excitation while the last term is the quadratic damping.

The boundary conditions for a beam with nonlinear support flexibility at one end are

$$\frac{\partial \hat{v}}{\partial \hat{s}}(0, \hat{t}) = 0, \quad EI\frac{\partial^2 \hat{v}}{\partial \hat{s}^2}(0, \hat{t}) = \kappa_1 \frac{\partial \hat{v}}{\partial \hat{s}}(0, \hat{t}) + \kappa_3 \left(\frac{\partial \hat{v}}{\partial \hat{s}}\right)^3,$$

$$\frac{\partial^2 \hat{v}}{\partial \hat{s}^2}(L, \hat{t}) = 0, \quad \frac{\partial^3 \hat{v}}{\partial \hat{s}^3}(L, \hat{t}) = 0 \tag{2}$$

where κ_1 and κ_3 represent the linear and cubic rotational stiffness coefficients, respectively. The limiting cases for an elastically restrained support at one end are the clamped-free (infinite stiffness) and pinned-free (zero stiffness) boundary conditions.

The next step is to nondimensionalize the equation of motion and boundary conditions. Nondimensionalization allows for greater generality and simplicity in the analysis at the same time. We choose to nondimensionalize the variables according to the following scheme:

$$s = \frac{\hat{s}}{L}, \quad v = \frac{\hat{v}}{L}, \quad t = \hat{t}\sqrt{\frac{EI}{mL^4}}, \quad \tilde{\mu} = \hat{\mu}\frac{L^2}{\sqrt{mEI}}, \quad \tilde{c} = \hat{c}\frac{L}{m}, \quad \tilde{\Omega} = \hat{\Omega}\sqrt{\frac{mL^4}{EI}}, \quad \tilde{a}_b = \hat{a}_b\frac{mL^3}{EI}. \tag{3}$$

Using these variables, we rewrite Eq. (1) as

$$\ddot{v} + \tilde{\mu}\dot{v} + v'''' = -\left(v'(v'v'')'\right)' - \frac{1}{2}\left(v'\int_1^s \left(\int_0^s (v')^2\,\mathrm{d}s\right)^{\cdot\cdot}\mathrm{d}s\right)' + \tilde{a}_b\cos(\tilde{\Omega}t) - \tilde{c}|\dot{v}|\dot{v}. \tag{4}$$

We perform another scaling of the equation of motion and the boundary conditions. The purpose of this scaling is to reduce the numerical values of the nonlinear coefficients and help in the ordering of the terms for application of the perturbation method. The scaling factor z_n will be related to a linear natural frequency of the system. The relationship is set to be $\omega_n = z_n^2$ so that the natural frequency of interest will become unity. The two independent variables are scaled according to $s^* = z_n s$ and $t^* = z_n^2 t$. Using these scalings, we find that the equation of motion becomes

$$\ddot{v} + \frac{\tilde{\mu}}{z_n^2}\dot{v} + v'''' = \frac{\tilde{a}_b}{z_n^4}\cos\left(\frac{\tilde{\Omega}}{z_n^2}t\right) - \tilde{c}|\dot{v}|\dot{v} - z_n^2\left(v'(v'v'')'\right)' - \frac{z_n^2}{2}\left(v'\int_{z_n}^s \left(\int_0^s v'^{\,2}\,\mathrm{d}s\right)^{\cdot\cdot}\mathrm{d}s\right)' \tag{5}$$

where the prime and overdot denote spatial and time derivatives, respectively, and the asterisk superscript has been dropped. The oundary conditions become

$$v''(1, t) = 0, \quad v'''(1, t) = 0, \quad v(0, t) = 0, \quad v''(0, t) = \tilde{\alpha}_1 v'(0, t) + \tilde{\alpha}_3 v'(0, t)^3 \tag{6}$$

where

$$\tilde{\alpha}_1 = \frac{\kappa_1 L}{EI} \quad \text{and} \quad \tilde{\alpha}_3 = \frac{\kappa_3 L}{EI}.$$

6. Perturbation solution

As in most nonlinear continuous systems, Eq. (5) subject to Eq. (6) is not amenable to a closed-form solution. The ability to model the diverse dynamics embedded in such equations by analytical functions might not be feasible. At this point, a solution can be obtained via numerical methods for a very specific set of parameter values. With each change in the numerical value of a parameter, the equations subject to the boundary conditions must be integrated anew. To develop any sort of parameter sensitivity or bifurcation analysis would be computationally unwieldy. However, perturbation methods offer an alternate approach that can provide qualitative insight in addition to reliable quantitative results in a relatively simple fashion.

6.1. Method of multiple scales

As the name implies, the method of multiple scales takes advantage of the scaling that appears to be inherent in nature. This scaling can take many forms, but for problems of our interest, time is the focus. This method takes advantage of the time scaling involved in the occurrence of nonlinear phenomena in systems.

To apply the method of multiple scales requires that the equation of motion be in a suitable form. The nondimensionalizations carried out in the earlier part of this paper were part of this process. One final scaling is necessary. This involves defining the remaining parameters in terms of a small parameter ε. This parameter will act as a convenient expansion parameter and determine the ordering of the various terms in the equation.

Defining

$$\frac{\tilde{\mu}}{z_n^2} = \varepsilon^2 \mu, \quad \frac{\tilde{a}_b}{z_n^4} = \varepsilon^3 a_b, \quad \frac{\tilde{\Omega}}{z_n^2} = \Omega, \quad \tilde{c} = \varepsilon c$$

leads to

$$\ddot{v} + \varepsilon^2 \mu \dot{v} + v^{iv} = \varepsilon^3 a_b \cos(\Omega t) - \varepsilon c \dot{v}|\dot{v}| - z_n^2 \left[v'(v'v'')' \right]' - \frac{1}{2} z_n^2 \left[v' \int_{z_n}^{s} \left(\int_0^s v'^{\,2}\, \mathrm{d}s \right)^{\cdot\cdot} \mathrm{d}s \right]' \tag{7a}$$

subject to

$$v(0,t) = 0, \quad v''(z_n,t) = 0, \quad v'''(z_n,t) = 0, \quad v''(0,t) = \alpha_1 v'(0,t) + \alpha_3 v'(0,t)^3 \tag{7b}$$

where

$$\alpha_1 = \frac{\kappa_1 L}{EI z_n} \quad \text{and} \quad \alpha_3 = \frac{\kappa_3 L z_n}{EI}. \tag{8}$$

Now the foundation of the method of multiple scales is that time t can be broken down into a succession of independent time scales given by the relationship $T_n = \varepsilon^n t$ (Nayfeh, 1981). The parameter ε can also serve as an expansion parameter for the dependent variable. The form of the expansion is

$$v(s, T_0, T_1, \ldots; \varepsilon) = \varepsilon v_1(s, T_0, T_1, \ldots; \varepsilon) + \varepsilon^2 v_2(s, T_0, T_1, \ldots; \varepsilon) + \varepsilon^3 v_3(s, T_0, T_1, \ldots; \varepsilon) + \cdots \tag{9}$$

and the time derivatives become

$$\frac{\partial}{\partial t} = \frac{\partial}{\partial T_0} + \varepsilon\frac{\partial}{\partial T_1} + \varepsilon^2\frac{\partial}{\partial^2 T_2} + \cdots = D_0 + \varepsilon D_1 + \varepsilon^2 D_2 + \cdots \tag{10a}$$

and

$$\frac{\partial^2}{\partial t^2} = D_0^2 + 2\varepsilon D_0 D_1 + \varepsilon^2 D_1^2 + 2\varepsilon^2 D_0 D_2 + \cdots \tag{10b}$$

The procedure is to substitute Eqs. (9), (10a) and (10b) into Eqs. (7a) and (7b). Then the coefficient of each power of ε is set equal to zero. The result is a hierarchy of linear equations and associated boundary conditions. Restricting our analyses to the first three orders, we have the following:

Order ε:

$$D_0^2 v_1 + v_1^{iv} = 0$$

$$v_1(0, t) = 0, \quad v_1''(z_n, t) = 0, \quad v_1'''(z_n, t) = 0, \quad v_1''(0, t) = \alpha_1 v_1'(0, t) \tag{11}$$

Order ε^2:

$$D_0^2 v_2 + v_2^{iv} = -2D_0 D_1 v_1$$

$$v_2(0, t) = 0, \quad v_2''(z_n, t) = 0, \quad v_2'''(z_n, t) = 0, \quad v_2''(0, t) = \alpha_1 v_2'(0, t) \tag{12}$$

Order ε^3:

$$D_0^2 v_3 + v_3^{iv} = -2D_0 D_1 v_2 - 2D_0 D_1 v_1 - \mu D_0 v_1 - D_1^2 v_1 - z_n^2\left(v'(v'v'')'\right)' - \frac{z_n^2}{2}\left[v'\int_{z_n}^{s}\int_{0}^{s}(v'^2\,\mathrm{d}s)^{\cdot}\,\mathrm{d}s\right]' + a_b\cos(\Omega t)$$

$$v_3(0, t) = 0, \quad v_3''(z_n, t) = 0, \quad v_3'''(z_n, t) = 0, \quad v_3''(0, t) = \alpha_1 v_3'(0, t) + \alpha_3 v_3'(0, t)^3. \tag{13}$$

Beginning with the first-order equation and boundary conditions, Eq. (11), we seek a solution. This solution then allows consideration of the next order equation, and so on. The first-order equation is the linear problem and this is what we turn to next.

6.2. First-order equation

The first-order equation, with boundary conditions, Eq. (11), is a linear problem whose solution is assumed in the following separable form:

$$v_1(s, T_0, \ldots; \varepsilon) = \sum_{m=1}^{\infty}\left[\varphi_m(s)A_m(T_1, \ldots)\mathrm{e}^{i\omega_m T_0} + cc\right] \tag{14a}$$

where cc is the complex conjugate of the preceding term, $\omega_m = z_m^2/z_n^2$, and $\varphi_m(s)$ is the linear mode

shape. The linear mode shape for a free-elastically restrained beam (Chun, 1972) can be expressed as

$$\varphi_m(s) = -\alpha_1\gamma(\cos(s) - \cosh(s)) + \gamma(\sin(s) + \sinh(s)) + (\sin(s) - \sinh(s)) \tag{14b}$$

where

$$\alpha_1 = \frac{\sin(z_n)\cosh(z_n) - \cos(z_n)\sinh(z_n)}{1 + \cosh(z_n)\cos(z_n)}, \tag{14c}$$

$$\gamma = \frac{1+p}{1-p},$$

and

$$p = \frac{\cosh(z_n)\cos(z_n) - \sinh(z_n)\sin(z_n) + 1}{\cos(z_n)\cosh(z_n) + \sinh(z_n)\sin(z_n) + 1}.$$

The orthogonality condition for the linear mode shapes is

$$\int_0^{z_n} \varphi_m(s)\varphi_n(s)\,\mathrm{d}s = \delta_{mn} z_n$$

where δ_{mn} is the Dirac delta function.

Since we are considering a single-mode response, only a one-term expansion of Eq. (14a) will be considered, specifically, that consisting of the directly excited fourth mode ($m = 4$); that is,

$$v_1 = A_4\varphi_4(s)\mathrm{e}^{iT_0} + cc \tag{14d}$$

This is an assumption that the other modes of the beam do not significantly affect the motion of the beam and that only the directly excited-mode determines the type of motion being observed (Nayfeh and Mook, 1979).

6.3. Solvability conditions

Moving onto the second-order problem, we substitute Eq. (14a) into Eq. (12) and obtain

$$D_0^2 v_2 + v_2^{iv} = -2D_1 A_4 i\varphi_4 \mathrm{e}^{iT_0}$$

where $\omega_4 = 1$. The solution at each order must insure uniformity of the expansion (9). This is known as the *solvability condition* and will be presented in more detail for the third-order problem. For now we state that the solvability condition together with the orthogonality condition leads to $D_1 A_4 = 0$ which implies that the coefficient A_4 is not a function of T_1. It can be determined by imposing the solvability condition for the third-order problem. So v_2 is trivial.

At this point, it is prudent to introduce a detuning parameter σ that is a measure of the nearness of the forcing frequency to the frequency of the fourth mode. It is defined according to the relation: $\Omega = \omega_4 + \varepsilon^2\sigma$.

For the solution of the third-order problem, Eq. (13), we assume that

$$v_3 = V_3(s, T_2, \ldots)\mathrm{e}^{iT_0} + cc. \tag{15}$$

We substitute Eqs. (15) and (14d) into Eq. (13), recall that $v_2 = 0$, and arrive at

$$-V_3 + V_3^{iv} = \mathbf{H}$$

$$V_3(0, T_2) = 0, \quad V_3''(z_4, T_2) = 0, \quad V_3'''(z_4, T_2) = 0, \quad V_3''(0, T_2) = \alpha_1 V_3'(0, T_2) + 3\alpha_3 \varphi'^{\,3}_4 A_4^2 \bar{A}_4 \tag{16}$$

where

$$\mathbf{H} = -\mu i \varphi_4 A_4 - 2i\varphi_4 D_2 A_4 - 3z_4^2\left[\varphi_4'\left(\varphi_4'\varphi_4''\right)'\right]' A_4^2 \bar{A}_4 + 2z_n^2\left(\varphi_4' \int_{z_n}^{s}\int_0^{s} \varphi'^{\,2}_4 \, \mathrm{d}s \, \mathrm{d}s\right)' A_4^2 \bar{A}_4$$

$$+ a_b \cos(\Omega t) \mathrm{e}^{-iT_0}.$$

The solvability condition insures uniformity of the expansion of the dependent variable; it is found by using the concept of adjoint. To begin, the first of Eq. (16) is multiplied by the adjoint Ψ and integrated as follows:

$$\int_0^{z_n} \Psi\left(-V_3 + V_3^{iv}\right) \mathrm{d}s = \int_0^{z_n} \Psi \mathbf{H} \, \mathrm{d}s. \tag{17}$$

To determine the adjoint problem, we follow the procedure outlined in Ref. (Nayfeh, 1981) and find that the third-order problem is self-adjoint; that is, $\Psi = \varphi_4$. Consequently, the solvability condition becomes

$$\int_0^{z_4} \varphi_4 \mathbf{H} \, \mathrm{d}s - 3\alpha_3 \varphi'^{\,4}_4(0) A_4^2 \bar{A}_4 = 0. \tag{18}$$

Integrating Eq. (18) and applying the polar transformation $A_4 = \frac{1}{2} a_4 \mathrm{e}^{i\beta_4}$, we obtain the following *modulation equations* governing the amplitude and phase of the fourth mode:

$$a_4' = -\frac{1}{2}\mu a_4 + \frac{a_b}{z_4}\sin\vartheta - \check{c} a_4^2$$

$$a_4 \vartheta' = a_4 \sigma + \frac{1}{8}\delta_1 a_4^3 + \frac{a_b}{z_4}\cos\vartheta \tag{19}$$

where $\vartheta = \sigma T_2 - \beta_4$ and δ_1 denotes the effective nonlinear coefficient (excluding damping) in the solvability condition, Eq. (18). It is given by

$$\delta_1 = \int_0^{z_4}\left[-3z_4^2\left(\varphi_4'\left(\varphi_4'\varphi_4''\right)'\right)' + 2z_4^2\left(\varphi_4' \int_{z_4}^{s}\int_0^{s} \varphi'^{\,2}_4 \, \mathrm{d}s \, \mathrm{d}s\right)'\right]\varphi_4 \, \mathrm{d}s - 3\alpha_3 \varphi'^{\,4}_4(0), \tag{20}$$

To study the solutions of Eq. (19), we begin with the constant solutions (fixed points), which correspond to periodic motions of the beam. To this end, we set the time variation of the amplitude and phase in Eq. (19) equal to zero. The stability of the fixed points can be found by investigating the eigenvalues of the Jacobian of Eq. (19). It follows from Eq. (20) that if we neglect the contribution of the nonlinear torsional spring and consider only a clamped-free beam, the sign of the nonlinear coefficient is determined by the relative contributions of the nonlinear curvature and inertia terms. For the first mode, the nonlinear curvature term dominates and the frequency-response curve will display a hardening-type behavior. For higher modes, the nonlinear inertia term is larger than the nonlinear curvature term and, therefore, the frequency-response curve displays a softening- type behavior.

Inclusion of the nonlinear (cubic) elastic element at the boundary allows for the further hardening (or softening) of the frequency-response curve, depending on whether the nonlinear stiffness coefficient is negative (or positive).

Solving for the fixed points, we set the right-hand side of Eq. (19) equal to zero. Using some algebraic manipulations, we reduce the two equations to one single equation known as the *frequency-response equation* written as

$$\left[\left(\frac{1}{2}\mu + \check{c}a_4\right)^2 + \left(\sigma + \frac{1}{8}\delta_1 a_4^2\right)^2\right] a_4^2 = \frac{a_b^2}{z_4^2}. \tag{21}$$

For most of our experiments, the detuning parameter and the forcing amplitude comprise the control parameters. Fixing one control parameter while varying the other provides a set of plots that detail the pattern of behavior of the fixed points (i.e., periodic motions of the beam). In the following sections, we compare theoretical and experimental results for such plots for a response consisting of the fourth mode of the beam.

7. Clamped-free boundary conditions

In this section, we attempt to match the experimental results with the above theoretical analysis. The

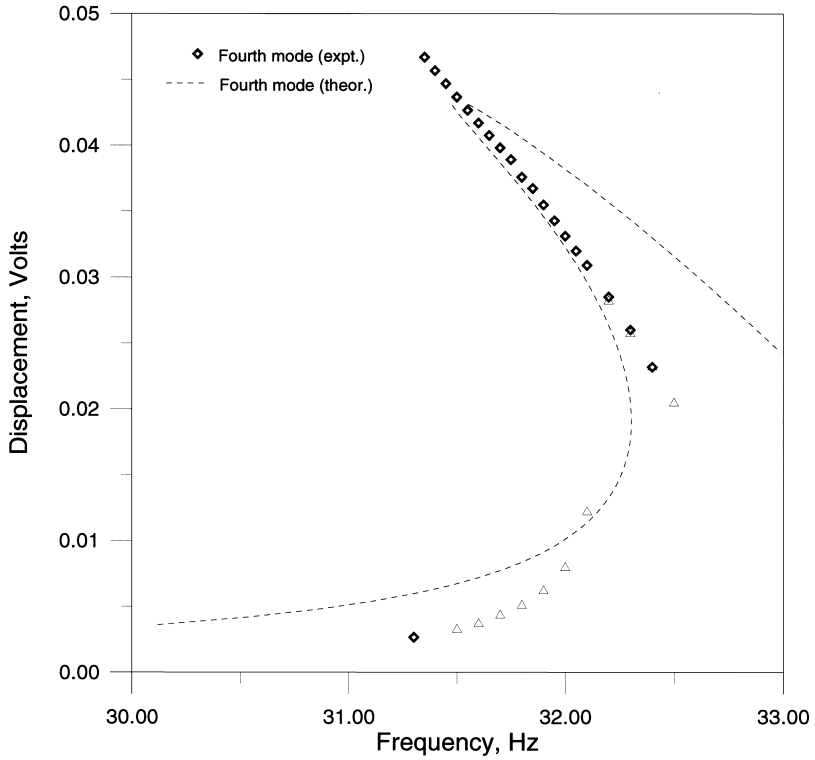

Fig. 2. Experimentally and theoretically (clamped-free ends) obtained frequency-response curves for an excitation amplitude of 0.7 *g*.

experimental results of the fourth-mode responses of the horizontal beam are shown in Fig. 2. The theoretical results involve the assumption of a perfectly clamped end. The comparison may reveal deficiencies in the model and/or experiment.

For the experimental results, we consider the fourth-mode response ($z_4 \approx 10.996$) of the horizontal cantilever beam, specifically, the frequency-response curves for an excitation amplitude of 0.7 g and the amplitude-response curves for an excitation frequency of 32.00 Hz. Assuming clamped-free conditions in the analysis, we find that $\delta_1 \approx 7557$ ($\approx 7952 - 395$), which combines the contributions from the inertia nonlinearity (-395) and the curvature nonlinearity (7952). From the half-power point, we find that the damping ratio $\hat{\xi} = 0.001$. Fig. 2 shows a comparison between the theoretically (Eq. (21)) and experimentally obtained frequency-responses curves. Two discrepancies were found. The first (not shown) is that the frequency–response curve with only a linear viscous damping term exhibited a jump down frequency very far from the experimental jump down frequency. The inclusion of quadratic damping allowed for a curve fitting process whereby the jump down frequency for the theoretical results was forced to match that of the experimental results by choosing an appropriate quadratic damping coefficient. The addition of the quadratic damping for a blunt body is physically reasonable as the large deflections observed during the experiment most probably gave rise to significant air damping, which is proportional to the square of the velocity. The second obvious discrepancy is the difference in the slopes of the theoretically and experimentally obtained frequency-response curves. The experimentally obtained frequency-response curve is softer than the theoretically obtained frequency-response curve. This implies that the nonlinear coefficient δ_1 requires modification. Possible sources of this revision are discussed in the next section.

8. Error analysis

The difference in the slopes of the experimentally and theoretically obtained frequency-response curves may have several sources. Each source may affect either the experimental or theoretical results. We note that, in a comparison between experimental and theoretical results, sometimes it is taken for granted that the experimental results are the correct ones and that one should strive to match theory to experiment. However, it may happen that the experimental results will need to be adjusted. Errors in measurement, transducer placement, and faulty calibration curves are just a few of the possible sources of error in experimental measurements (Wilson, 1996; Dally et al., 1993). We hypothesize three possible sources that may be responsible for the discrepancy, namely,

1. nonlinear strain gage calibration curve,
2. midplane stretching, and
3. nonlinear stiffness at the clamped boundary.

The nonlinear strain gage calibration curve may be due to unusually large strains induced by vibrations of the beam. This would most likely harden the experimental data points, thereby bringing them closer to the theoretical results. From the literature and manufacturer information, this source was found to be an unlikely culprit. Attempts to obtain a dynamic calibration curve for the fourth mode by placing an accelerometer on the beam to provide displacement related measurements in conjunction with strain measurements proved inconclusive. Also such measurement may include the effect of the second possible error source, midplane stretching. The theoretical development is based on the assumption of inextensionality of the midplane of the beam. This is found to be very adequate for beams with one end unrestrained. However, it is an assumption and possibly, under very large deflections and curvatures, the midplane stretching effect may become important. This effect was much harder to measure and, once

again, a search through the literature on this topic made the likelihood of midplane stretching very small. The inclusion of midplane stretching would have hardened the theoretical results.

Finally, consideration of a nonideal-clamping boundary led us to perform an exploratory experiment whereby two small accelerometers were placed on the clamping fixture. One was centered while the other was placed close to the edge of the clamp, on the side where the beam was extending out. As forcing frequency and amplitude sweeps were performed, we observed a significant relative change in acceleration levels between the two transducers. At low levels, the accelerations matched quite well, while during large-amplitude motions the accelerometer closer to the edge displayed larger values than those displayed by the center accelerometer. Note that all motions were restricted to unimodal responses consisting of the fourth mode. A comparison of the readings of the center and edge accelerometers revealed a hardening-type behavior. Therefore, the inclusion of a hardening-type spring at the clamped end would appear to be the most viable explanation of the difference between the experimentally and theoretically obtained frequency-response curves. As a qualifying insight, the difference in acceleration levels may be due to flexure of the metallic clamping fixture and/or rotation of the shaker armature to which the clamping fixture is attached. From our experience in the laboratory, the latter is the more likely source. However, from a modeling point of view, the mathematical formulation is the same for both. So in the next section, we refine our analysis to include boundary flexibility and re-examine the results vis-a-vis the experimental data.

9. Nonideal clamps

Next we consider the case of a torsional spring with linear and cubic stiffness terms in the theoretical analysis. By incorporating the boundary flexibility, we have introduced two additional unknowns into our analysis, the linear and cubic stiffness coefficients. The linear stiffness coefficient can be found by taking the first experimentally obtained linear natural frequency and substituting it into Eq. (14c). Then we deduce the value of the cubic stiffness term by curve fitting the theoretically obtained frequency-response curve for one excitation amplitude. Again, we use the experimental jump down frequency to ascertain the value of the quadratic-damping coefficient. Once these parameters are determined, we check whether the remaining theoretically obtained frequency- and amplitude-response curves match the experimentally obtained curves. Reasonable agreement will thereby lend credibility to the assertion that the previously observed discrepancy is attributable to a nonideal-clamping boundary.

First, we need to estimate the linear stiffness coefficient. The value for α_1 is found by improving the agreement between the theoretically and experimentally obtained linear natural frequencies. We find that a change in the value of the linear stiffness term only affects the second decimal of z_4 (Blevins, 1979). As such, we chose $z_4 \approx 10.977$ as a value that best fit the first four natural frequencies of our beam. This choice gives $\alpha_1 z_n \approx 581$. Next we consider the frequency-response curve for an excitation amplitude of 0.7 g. Performing the curve fitting, we find that we can match the theoretically and experimentally obtained frequency-response curves as shown in Fig. 3. We find the value for the quadratic damping coefficient, $\hat{c} \approx 0.33$, from the curve fitting the jump down frequency of the theoretical model to the experimentally obtained jump down frequency and $\delta_1 \approx 4560$ from the curve fitting the backbone curve of the experimentally obtained frequency-response curve and using this value for the theoretical model. Using these values and Eqs. (8) and (20), we can then estimate that $\alpha_3 \approx 10^7$. From the half-power point method, we find $\mu \approx 0.0003$. Using these values, we obtain an equally excellent match between the experimentally and theoretically obtained frequency-response curves for an excitation amplitude of 0.9 g as shown in Fig. 4. As an additional boost to confidence, we compare the theoretically and experimentally obtained amplitude-response curves in Fig. 5 for an excitation frequency of 32 Hz. Again a fairly good match is realized. A final fine tuning was performed where the forcing amplitude was

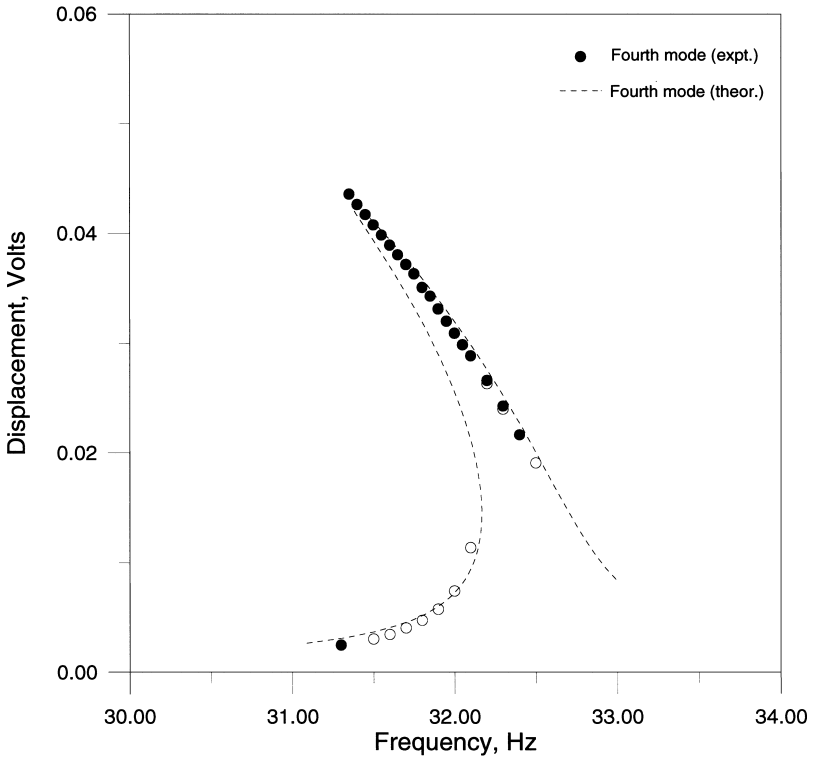

Fig. 3. Experimentally and theoretically (spring-hinged-free end) obtained frequency-response curves for an excitation amplitude of 0.7 g.

adjusted. It was found that a 10% reduction in the forcing amplitudes improved the agreement. The physical explanation for this apparent energy loss is that the measured input signal is from the accelerometer placed on the clamping fixture. This signal is then transformed into the frequency domain by the dynamic signal analyzer. The magnitude of the peak in the spectrum at the forcing frequency is then assumed to be the total forcing amplitude. However, some structural feedback to the shaker occurs at the same frequency, which would result in an observed increase in the magnitude of the forcing. The contributions from these different sources cannot be separated in the frequency domain. Therefore, the actual force imparted to the beam by the shaker is lower.

Since the choice of the expansion parameter affects the coefficients of the terms in the expansion, a final step is required. The forcing frequency, forcing amplitude, and linear viscous damping were the experimentally obtained parameters that were fed into the theoretical model by scaling the values according to the transformations outlined in previous sections. However, the scalings and perturbation solution require a numerical value for one last parameter, the perturbation parameter ε. Though in some cases, the perturbation parameter is a physical variable, in this case, it is only an expansion parameter whose choice is not entirely arbitrary. For this case, we chose $\varepsilon \approx 0.01$. To complete the perturbation analysis, we need to evaluate the smallness of our perturbation terms based on our particular choice of the perturbation parameter. We use the chosen value of the perturbation parameter to check that the ratio $(\kappa_3/\kappa_1)\varepsilon^2 \ll 1$ is satisfied to insure the validity of our perturbation expansion. Using the estimated

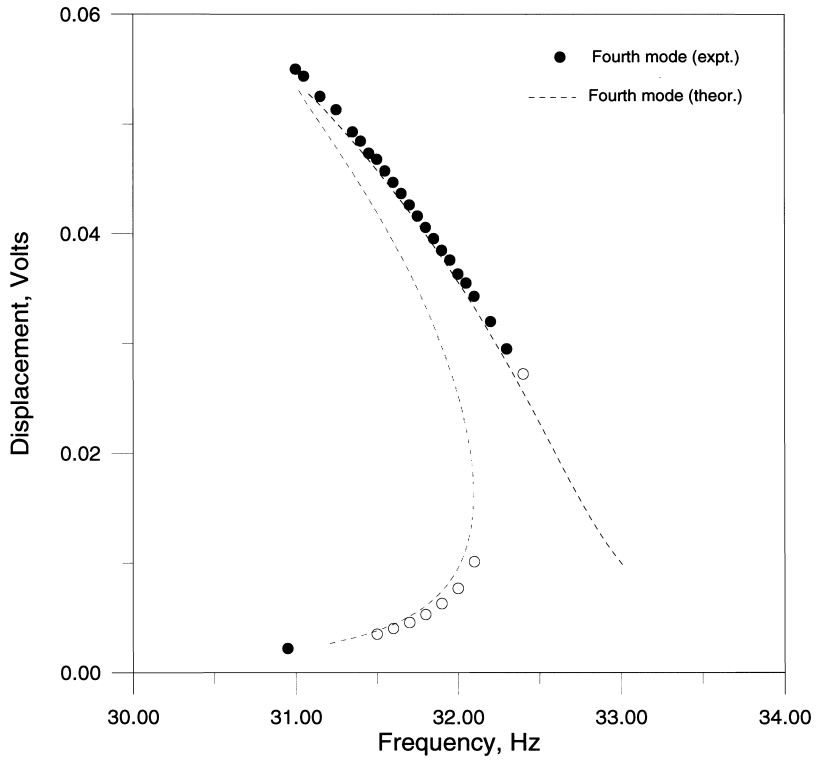

Fig. 4. Experimentally and theoretically (spring-hinged-free ends) obtained frequency-response curves for an excitation amplitude of 0.9 g.

values for the boundary stiffness coefficients, we find that $(\kappa_3/\kappa_1)\varepsilon^2 \approx (\alpha_3/\alpha_1 z_n^2) \approx 0.01$. If this check had failed, then a smaller value of the perturbation parameter would have been needed.

An alternate procedure for checking the validity of perturbation expansion would involve comparing the multiple-scales solution with a solution obtained by integrating the original differential equation.

10. Summary

The unimodal dynamics of a cantilever beam subjected to a harmonic external excitation was examined both experimentally and theoretically for the fourth mode. The experimentally obtained frequency-response curves exhibit hardening-type nonlinearity. However, in a comparison with the theoretical analysis for an ideal clamp, we found a large discrepancy. This discrepancy was found to be due to two sources: air damping and boundary flexibility. The source of the boundary flexibility can be attributed to clamping flexibility and/or lateral displacements of the shaker armature. The air damping was modeled by adding a quadratic damping term while the boundary flexibility was modeled by replacing the clamped end boundary condition by a torsional spring. This rotational elastic element possesses linear and cubic stiffness components. The addition of these two elements to our model was found to improve dramatically the agreement between the experimentally and theoretically obtained frequency- and amplitude- response curves.

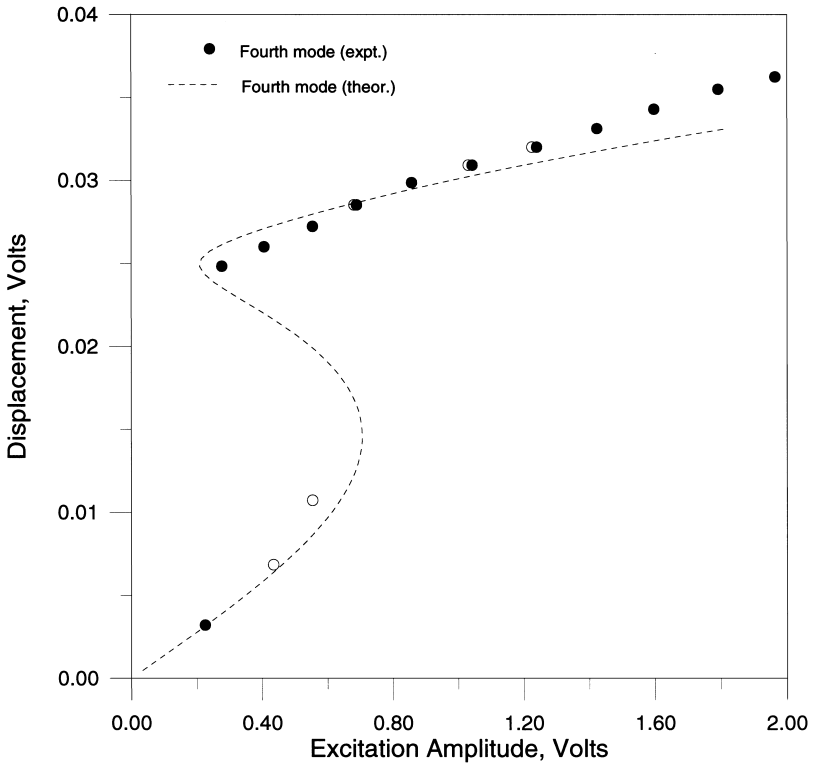

Fig. 5. Experimentally and theoretically (spring-hinged-free ends) obtained amplitude-response curves for an excitation frequency of 32.00 Hz.

Acknowledgements

The author would like to acknowledge the tremendous insight and compassion of Dr. Ali H. Nayfeh. Furthermore, the author would be remiss not to mention the down in the trenches, everyday help of Dr. Jon Pratt (NIST) and Wayne Kreider. Finally, the author extends his deepest thanks for the insightful comments and suggestions of the reviewers.

References

Anderson, T.J., Nayfeh, A.H., Balachandran, 1996. Experimental verification of the importance of the nonlinear curvature in the response of a cantilever beam. Journal of Vibration and Acoustics 118, 21–27.

Berdichevsky, V.L., Kim, W.W., Ozbek, A., 1995. Dynamical potential for nonlinear vibrations of cantilevered beams. Journal of Sound and Vibration 179, 151–164.

Blevins, R.D., 1979. Formulas for Natural Frequency and Mode Shape. Van Nostrand Publishers, New York.

Boutaghou, Z.E., Erdman, A.G., 1989. On the dynamics of Timoshenko/Euler–Bernoulli beams: a unified approach. ASME Design Engineering 18 (3), 69–73.

Chun, K.R., 1972. Free vibration of a beam with one end spring-hinged and the other free. Journal of Applied Mechanics 39, 1154–1155.

Crespo da Silva, M.R.M., 1991. Equations for nonlinear analysis of 3D motions of beams. Applied Mechanics Review 44, S51–59.

Crespo da Silva, M.R.M., Glynn, C.C., 1978a. Nonlinear flexural–flexural–torsional dynamics of inextensional beams. Part I: Equations of motion. Journal of Structural Mechanics 6, 437–448.

Crespo da Silva, M.R.M., Glynn, C.C., 1978b. Nonlinear flexural–flexural–torsional dynamics of inextensional beams. Part II: Forced motions. Journal of Structural Mechanics 6, 449–461.

Dally, J.W., Riley, W.F., McConnell, K.G., 1993. Instrumentation for Engineering Measurements. Wiley, New York.

Donnell, L.H., 1976. Beams, Plates, and Shells. McGraw-Hill, New York.

Dowell, E.H., Traybar, J., Hodges, D.H., 1977. An experimental–theoretical correlation study of nonlinear bending and torsion deformations of a cantilever beam. Journal of Sound and Vibration 50, 533–544.

Gorman, D.J., 1975. Free Vibration Analysis of Beams and Shafts. Wiley, New York.

Haering, W.J., Ryan, R.R., Scott, R.A., 1992. A new flexible body dynamic formulation for beam structures undergoing large overall motions. In: Proceedings of the 33rd Structures, Structural Dynamics, and Materials Conference, Dallas, TX.

Hodges, D.H., 1984. Proper definition of curvature in nonlinear beam kinematics. AIAA Journal 22, 1825–1827.

Hodges, D.H., 1987a. Finite rotation and nonlinear beam kinematics. Vertica 11, 297–307.

Hodges, D.H., 1987b. Noninear beam kinematics for small strains and finite rotations. Vertica 11, 573–589.

Hodges, D.H., Crespo da Silva, M.R.M., Peters, D.A., 1988. Nonlinear effects in the static and dynamic behavior of beams and rotor blades. Vertica 12, 243–256.

Love, A.E.H., 1944. A Treatise on the Mathematical Theory of Elasticity. Dover, New York.

McConnell, K.G., 1995. Vibration Testing. Wiley, New York.

Moon, F.C., Holmes, P.J., 1985. Double-poincare sections of a quasi-periodically forced chaotic attractor. Physical Letters A 111, 157–160.

Nayfeh, A.H., 1973. Perturbation Methods. Wiley, New York.

Nayfeh, A.H., 1981. Introduction to Perturbation Techniques. Wiley, New York.

Nayfeh, A.H., Balachandran, B., 1995. Applied Nonlinear Dynamics. Wiley, New York.

Nayfeh, A.H., Mook, D.T., 1979. Nonlinear Oscillations. Wiley, New York.

Nayfeh, A.H., Mook, D.T., Lobitz, D.W., 1974. Numerical–perturbation method for the nonlinear analysis of structural vibrations'. AIAA Journal 12, 1222–1228.

Nayfeh, A.H., Pai, P.F., 1996. Linear and Structural Mechanics. Wiley, New York.

Oden, J.T., Bathe, K.J., 1978. A commentary on computational mechanics. Applied Mechanics Review 31, 1053–1058.

Ostachowicz, W.M., Krawczuk, M., 1991. Analysis of the effect of cracks on the natural frequencies of a cantilever beam. Journal of Sound and Vibration 150, 191–201.

Pai, P.F., Nayfeh, A.H., 1990. Three-dimensional nonlinear vibrations of composite beams. Part I: Equations of motion. Nonlinear Dynamics 1, 477–502.

Pai, P.F., Nayfeh, A.H., 1992. A nonlinear composite beam theory. Nonlinear Dynamics 3, 273–303.

Suleman, A., Modi, V.J., Venkayya, V.B., 1995. Structural modeling issues in flexible systems. AIAA Journal 33, 919–923.

Tabaddor, M., 1996. Nonlinear Vibration of Beam and Multibeam Systems. Ph.D. Dissertation, Virginia Polytechnic Institute and State University, Blacksburg, VA.

Tabaddor, M., Nayfeh, A.H., 1997. An experimental investigation of multimode responses in a cantilever beam. Journal of Vibration and Acoustics 119 (4), 532–538.

Wilson, J., 1996. A Bit More (or Less) Accuracy? Test Engineering and Management, April/May, pp. 12–13.

Zavodney, L.D., Nayfeh, A.H., 1989. The non-linear response of a slender beam carrying a lumped mass to a principal parametric excitation: theory and experiment. International Journal of Non-Linear Mechanics 24, 105–125.